Color and Image Characterization of a Three CCD Seven Band Spectral Camera

Ana Gebejes, Joni Orava, Niko Penttinen, Ville Heikkinen,
Jouni Hiltunen, and Markku Hauta-Kasari

University of Eastern Finland, Institute of Photonics
P.O.BOX 111, 80101 Joensuu, Finland
{ana.gebejes,joni.orava,niko.penttinen,ville.heikkinen,jouni.hiltunen,
markku.hauta-kasari}@uef.fi

Abstract. In this study spectral and spatial characterization of a seven channel FluxData 1665 MS7 three-CCD spectral video camera was performed in terms of the sensor spectral sensitivity, linearity, spatial uniformity, noise and spatial alignment. The results indicate small deviation from ideal linear sensor response. Also, a small spatial non-uniformity and systematic shift exists between the channel images. However, images were observed to have high quality in term of noise. Spectral characterization showed that the sensor has good response in the 380-910 nm region with only some sensitivity limitations in the 715-740 nm range. We also evaluated the spectral reflectance estimation in 400-700 nm range using empirical regression methods and the Digital ColorChecker SG and ColorChecker charts. These experiments resulted in average $\Delta E00$ color accuracy of 1.6 – 2.4 units, depending on the illuminant and estimation method.

1 Introduction

Spectral imaging system is able to capture spectral information coming from the imaged scene with a certain number of spectral bands and image pixels.The output of such system is a spectral reflectance image that provides a representation of an object that is useful for object analysis and visualization. Therefore, spectral imaging is a useful technique in many field: remote sensing, astronomy, medicine and cultural heritage [1],[2],[3]. In several applications there is a need for monitoring via spectral video imaging. For example industrial production line inspections or medical applications. However, currently video output is possible only for sensors with relatively small number of spectral bands, due to hardware limitations.

Here we concentrate on characterization of one recently developed spectral video imaging system, FluxData 1665 MS7. This system is capable of acquiring seven band spectral video information with high spatial resolution and with short exposure times. The 30 fps video output makes this system a rapid acquisition tool when compared to other spectral imaging systems. Fast imaging, spatial properties and portability makes this device a practical spectral imaging system.

A. Elmoataz et al. (Eds.): ICISP 2014, LNCS 8509, pp. 96–105, 2014.

For instance the Liquid Crystal Tunable Filter (LCTF) systems require much longer exposure times due to losses in the tunable filter [4]. Using computational post processing, estimation of spectral radiance of illumination, reflectance of an object [5]-[8], and the radiance signal can be done for every pixel of the acquired image.

We performed a spectral and spatial characterization of the FluxData 1665 MS7 system focusing on spectral sensitivities, linearity, spatial uniformity, spatial sensor alignment and noise. Characterization of these properties provides information for the system calibration and its preparation for practical applications. We also performed spectral reflectance estimation in 400–700 nm for standard color chart data and used these estimates to calculate colorimetric representations under three standard illuminants (CIE D65, A and F11).

2 Camera Description

Table 1 summarizes the specifications of the seven channel FluxData 1665 MS7. The camera system uses the idea of dispersing the light by a trichroic prism assembly yet controlling the dispersed spectrum by interference filters coupled between the prisms. The trichroic prism assembly has high light efficiency and small amount of the incoming light will be absorbed by it making the assembly suitable for imaging with short exposure times. It splits the incoming light in three spectral compositions and directs it to three Charge-Coupled Devices (CCD). Each CCD has a separate Ethernet connection to a computer which allows sensor-wise exposure time control and data handling.

Table 1. Device specifications for FluxData 1665 MS7

Image device	Sony ICX285 - Basler scA1400 - 30gm/gc
Number of image devices	3 (2 Bayer BG color and 1 mono)
Number of Channels	7
Sensor size	1040 x 1392 px (Pixel Size: 6.45 x 6.45 m)
Bit depth	12-bit
Frame Rate	30 f/s
Wavelength range	380 - 1000 nm
Lens	Carl Zeiss Planar 1,4/50 ZF-IR

CCD1 and CCD2 are color sensors having conventional R, G and B filters organized in a Bayer pattern while CCD3 is a monochromatic sensor. After passing the lens system the incoming light is hitting the first interference filter that will pass through all the wavelengths up to 750 nm. From 750 nm up the all the wavelengths will be directed to CCD3. This way this sensor measures only the near infrared part of the incoming spectrum. The transmitted light continues to travel inside the prism until it hits the second interference filter. This is a band pass filter that passes through one band from 470 nm to 540 nm and one band from 620 nm to 730 nm. This light is directed to CCD2. The remaining two bands

(from 380 nm to 460 nm and 530 nm to 610 nm) are directed to CCD1. These are ideal theoretical values whereas the real filters do not have such sharp cut off wavelengths. All three sensors can be exposed simultaneously, and therefore the capture of the spectral information is possible with only a single shot.

3 Experimental Setup

In the experiments we performed the measurements using three different setups, to characterize the spectral, spatial and colorimetric properties of the system. The experimetal part of this work is presented in two subsections: Spectral and spatial characterizations and Spectral reflectance estimations.

3.1 Spectral and Spatial Characterizations

Spectral and spatial characterization includes the validation of the cameras spectral sensitivity, linearity, spatial uniformity, noise and spatial alignment. These five experiments can be summarized in two main experimental setups shown on Figure 1. Figure 1a shows the setup scheme used for the camera sensitivity measurements. It consists of a GigaHertz Optik Integrating Sphere of a diameter of 500 mm, monochromator with a halogen light source, Hamamatsu PMA-11 optical fiber spectrometer and the FD-1665-MS7. The camera was placed in front of the integrating sphere at a 0° angle and focused inside the sphere. The sphere was illuminated with the monochromator placed at a 45° and it was set to the wavelength range of 380 nm to 910 nm with a 5 nm wavelength step giving 107 wavelengths in total. For each wavelength the radiant flux was measured with the spectrometer and a seven channel image was acquired with the camera. Therefore, in these measurements all the elements in the optical path of the camera were included: optics, trichroic prism assembly with interference flters and the sensors. All the 107 wavelengths were measured and imaged one by one. The images were corrected for the black offset and denoising was performed by spatially averageing a 100x100 pixel area from the center of the image. The sensitivities were obtained by dividing the camera response for each channel with the measured radiant flux of the light.

To validate the linearity of the sensors the same setup was used (Figure 1a) only the monochromator and spectrometer were removed and a halogen light source was used to illuminate the sphere. The source was set to its maximum power and the exposure times for each channel were set so that the maximum of the sensor dynamics can be reached with no saturation. The power was then decreased by a step of 7% to get a total of 14 images for each channel. In addition, these images were used to evaluate the spatial uniformity and calculate the Signal-to-Noise Ratio (SNR) channel-wise. The SNR was calculated from these images using Equation 1.

$$\mathrm{SNR} = 20log_{10}\frac{S}{N} \tag{1}$$

where S is the mean of the brightest image of the integrating spheres field and N is the standard deviation of the same image. The results are presented in Table 2 and will be discussed in Section 3.

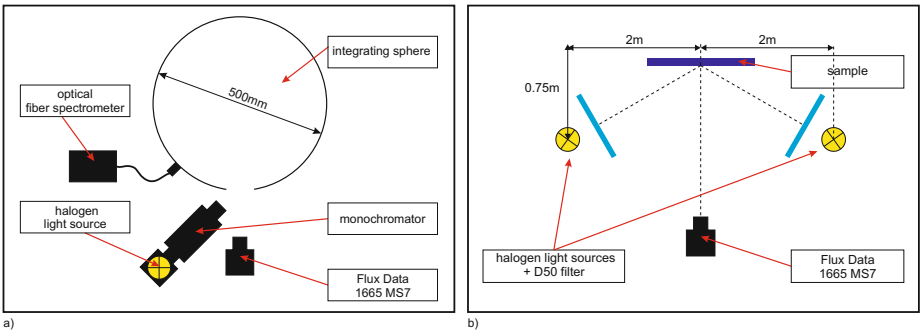

Fig. 1. a) Integrating sphere setup sheme and b) Image acquisition setup sheme

For the purpose of image acquisition the setup depicted on Figure 1b was used. The measuring geometry used was 70°/0°. The camera was placed in front of the sample at 0° to the normal of the sample. Two halogen light sources with a D50 filter were placed at 70° from the surface normal in order to uniformly illuminate the sample surface. D50 filter was used in order to achieve a spectrally more uniform light source. A seven channel image of a 24 patch ColorChecker Classic (CC24) was taken. The exposure time was set so that for each CCD the maximum of its dynamics can be used without saturation (aperture size f/8; exposure times: 350 ms,250 ms,300 ms for CCD1, CCD2 and CCD3 respectively). The distance of the camera was selected such that the whole area of CC24 can be enclosed. This image was used to evaluate the spatial alignment of the three sensors. For the evaluation purpose subtraction of images coming from different sensors was performed. As the CC24 has a checker board structure misalignment can be spotted at the edges of each patch as a shift of the image in certain direction.

3.2 Spectral Reflectance Estimations

Spectral reflectance estimation accuracy was evaluated using the Digital ColorChecker SG (SG) and CC24 charts. The FluxData measurements for these charts were performed in Spectralight III light booth using D65 light source and 45/0 (light./meas.) geometry. During the measurements, the camera settings were kept constant (aperture size f/5.6 and exposure time for each channel 50 ms). All the FluxData measurements were denoised using temporal average of 10 images and corrected for black offset. In addition, the spatial non-uniformities were corrected by dividing the measurements with the uniform reference white target values. As a final denoising step each patch was spatially averaged over area of 5x5 pixels.

The spectral reflectance factor data for the SG were measured in the light booth using PR 705 spectroradiometer in 380–780 nm and 2 nm sampling (45/0 light./meas. geometry). Interpolation with cubic spline was used to represent these data with 5 nm sampling. Spectral reflectance factor measurements for the CC24 chart was done using PerkinElmer 1050 spectrophotometer (8/0, light./meas.) and 350–1000 nm with 1 nm sampling.

We estimated the spectral reflectance factors of the chart color samples in 400–700 nm range using the empirical kernel based regression models ([6],[7]), so that we estimated the mapping $\mathbf{x} \rightarrow \mathbf{q}$, where the $\mathbf{x} \in \mathbb{R}^6$ is the FluxData measurement (6 bands in 400–700 nm range) and $\mathbf{q} \in \mathbb{R}^{61}$ is the corresponding spectral reflectance factor in 400–700 nm range with 5 nm sampling. In the estimations we used the empirical kernel based model presented in [6] and evaluated performance of the Matérn kernel [6] and first degree inhomogeneous polynomial kernel $\kappa(\mathbf{x}, \mathbf{z}) = \mathbf{x}^T\mathbf{z} + 1$, where $\mathbf{x}, \mathbf{z} \in \mathbb{R}^6$. First degree polynomial kernel was chosen, since in this case the estimation model corresponds to widely used (regularized/penalized) linear least squares fitting.

In the first evaluation we combined the SG (without the gray-scale borders, totally 96 samples) and CC24 (without black sample, totally 23 samples) sets and calculated the Leave-One-Out (LOO) result for this set of 119 samples, so that in each LOO step, the free parameters of models were optimized using the 10-fold cross-validation in training sets. As a second evaluation we used the 96 samples from the SG for training the estimation model and then evaluated the spectral reflectance estimation performance for the 23 samples from the CC24 chart. We evaluated the estimations in the test sets using the root-mean-square error (RMSE) and the Pearson Distance (PD) [6]. Evaluation of colorimetric accuracy of estimations were performed by using the $\Delta E00$ distance and CIE D65, A and F11 illuminants.

4 Results and Discussion

Figure 2 shows the seven spectral sensitivities measured both by the manufacturer and in this study. From the seven sensitivities the three marked as R1, G1 and B1 belong to CCD1, the three marked with R2, G2 and B2 belong CCD2 and the NIR belongs to CCD3. Due to the construction of the monochromator used the near infrared information was measured only until 910nm.

Table 2 summarizes the maximum wavelengths of each channel and Full Width Half Maximum (FWHM) values for the sensitivities measured in this work. The analysis of the obtained results shows that the curve maxima are at different level for some channels. Those channels are the ones on the edges of the cameras spectral range. In addition the shape of the main peak is not symmetrical with respect to the maximum for all channels and secondary peaks with low value maxima also exist. As they are coinciding with the maxima of other channels belonging to the same sensor they can be compensated if needed. Sensitivity limitations are observed in 715–740 nm range.

Assuming that the measurements performed by the manufacturer were performed under similar conditions and having all the elements in the optical path included a comparison of the measurements can be made. Differences in the location of the maxima, in the integral under the curves and the relative height of the maxima for some channels can be noted. The difference could arise due to possible difference in the camera assembly, calibration or a scaling factor with respect to the middle of the spectrum. In any case the results stress the need for sensor sensitivity measurements so that accurate camera calibration can be performed for a particular application and working conditions.

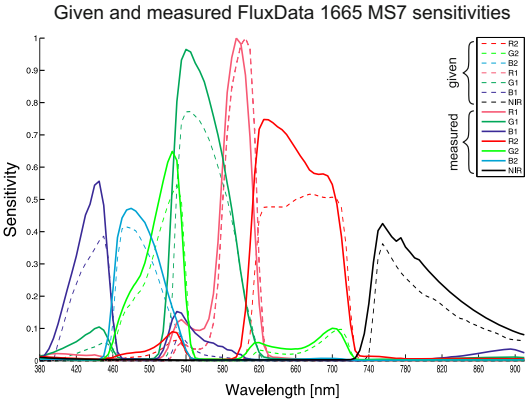

Fig. 2. Comparison between the measured sensitivities provided by the manufacturer (dashed lines) and the sensitivities measured in this work (bold lines)

Table 2. Spectral properties for each channel of the camera: top CCD R1, G1, B1; middle CCD R2, G2, B2 and bottom CCD - NIR

Channels	R1	G1	B1	R2	G2	B2	NIR
max wavelength [nm]	595	540	445	625	525	480	755
FWHM [nm]	40	60	40	100	40	60	80

Figure 3 summarizes the results of the linearity validation experiment sensorwise where Figure 3a correspond to CCD1, Figure 3b to CCD2 and Figure 3c to CCD3. Slight deviation from a straight line can be seen for all channels on CCD2 and CCD3. However, channel B1 deviates from a straight line the most.

Figure 4 shows seven uniformity map images of an integrating spheres field - channels R1, G1, B1, R2, G2, B2, NIR respectively. The images show that a difference in spatial uniformity between different sensors exists suggesting that a prism assembly introduces some non-uniformity. It can be also noted that the shape of R2, G2 and B2 are quite similar whereas R1, G1 and B1 are not.

The prism assembly could have some kind of incident angle and/or wavelength dependency so that with certain wavelength its transparency changes with incident angle.

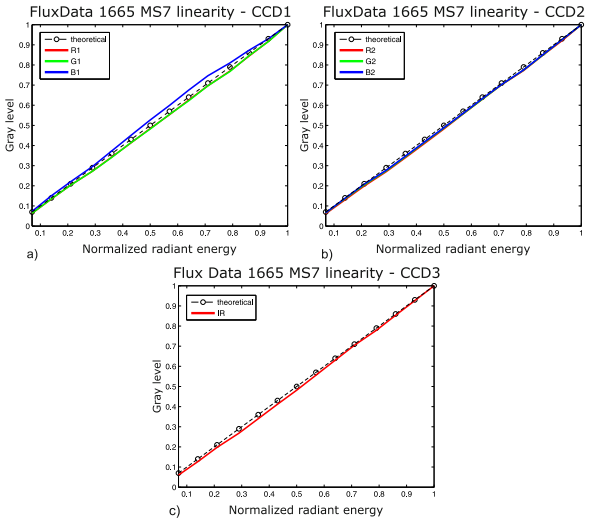

Fig. 3. a) linearity plot CCD1, b) linearity plot CCD2 and c) linearity plot CCD3

The largest spatial variation can be noticed for channels B1 and NIR as they are on the edges of the spectral range and they also happen to have the lower sensitivity maxima and SNR. However, this issue can be solved in post processing by dividing every acquired image with an image of a uniform white surface. Even though the non-uniformity has a small value it is present and for some applications it can be problematic as the values in the center of the image and on the edges of the image will be different. This stresses the need for a flat field correction in many applications.

Table 3 shows channel-wise Signal-to-Noise Ratio (SNR). Again it can be noted that the CCD2 is more consistent compared to CCD1 and channels B1 and NIR have lower values that could explain the larger spatial non-uniformity for those channels. However, the values for all channels are similar and the SNR of this magnitude represents excellent image quality.

Table 3. Channel-wise Signal-to-Noise Ratio

Channels	R1	G1	B1	R2	G2	B2	NIR
SNR [dB]	34	36	32	34	35	34	31

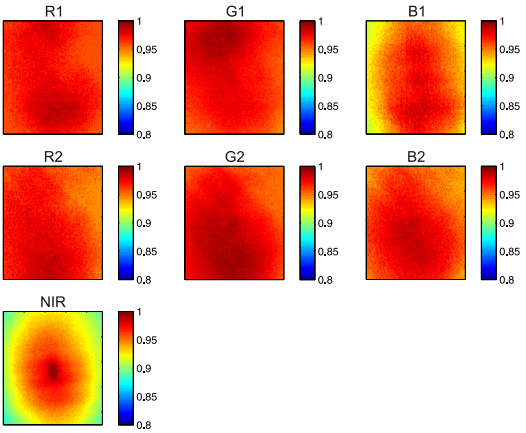

Fig. 4. Spatial uniformity maps of the seven channels integrating sphere field image R1, G1, B1, R2, G2, B2, NIR respectively

Figure 5 presents the image subtraction and shows an enlarged area of the CC24 lower left corner (first two gray patches) however similar behavior is observed for the whole image area. The images show a shift of the sensors leading to a misalignment of the seven images. In the case of CCD1 and CCD2 (Figure 5a) this shift is around 2 pixels horizontally and 1 pixel vertically. However, larger misalignment can be noted for CCD3. For CCD2 and CCD3 (Figure 5b) this shift is about 2 pixels horizontally and 6 pixels vertically while for CCD1 and CCD3 no horizontal shift but 6 pixels of vertical shift exists. In this experiment no distortions were noted but only a small and systematic shift. However, loss of the some pixel lines and columns will happen due to the correction.

Table 4 summarises the results of the reflectance estimation accuracy in terms of spectral (RMSE and PD) and color errors ($\Delta E00$ for CIE D65,A and F11 illuminants). Both the spectral and color errors suggest reasonable accuracy of the reflectance estimation. Average $\Delta E00$ color accuracy varies between 1.63 – 2.42 units, depending on the illuminant and estimation method. In most cases, the Matérn kernel shows significantly better performance when compared to the first degree polynomial kernel. Especially the maximum color error for the F11 illuminant is high, when the polynomial kernel is used. The relatively good

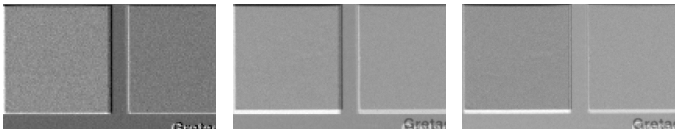

Fig. 5. Result of image subtraction: a) CC1 subtracted from CCD2, b) CC3 from CCD2, c) CC3 subtracted from CCD1

Table 4. Spectral reflectance factor (400–700 nm with 5 nm sampling) estimations for the SG (96 samples) and CC24 (23 samples) samples using FluxData 6 band measurements (in lightbooth with D65 source). Spectral and color errors for two evaluation cases using the first order inhomogeneous polynomial kernel and Matérn kernel. For each error type, the results correspond to Average/95^{th} percentile/Maximum values.

Method	RMSE	Pearson Distance	ΔE00 (D65)	ΔE00 (A)	ΔE00 (F11)
Leave-One-Out evaluation for SG & CC24 (119 samples)					
Polyn. kernel	0.0207/0.0357/0.0565	0.00461/0.0205/0.0398	1.89/4.38/6.91	1.82/4.07/5.60	2.42/6.01/11.67
Matérn kernel	0.0183/0.0366/0.0526	0.00270/0.0131/0.0259	1.64/3.68/7.06	1.63/3.40/7.04	1.90/4.59/6.98
Training set: SG, Test set: CC24 (23 samples)					
Polyn. kernel	0.0261/0.0352/0.0600	0.00389/0.0134/0.0173	1.94/3.83/4.06	1.96/3.69/3.91	2.42/4.43/5.87
Matérn kernel	0.0243/0.0379/0.0502	0.00275/0.0080/0.0096	1.85/3.45/3.53	1.86/3.31/3.32	2.12/4.02/4.04

performance of the Matérn kernel is partly due to the capability of this kernel to compensate for the non-linearities of the FluxData CCDs.

Figure 6 represents the visualisation of the estimates exibiting maximal spectral errors for Matérn kernel in terms of maximal RMSE value (top); maximal wavelengthwise error (middle) and maximal Pearson Distance.

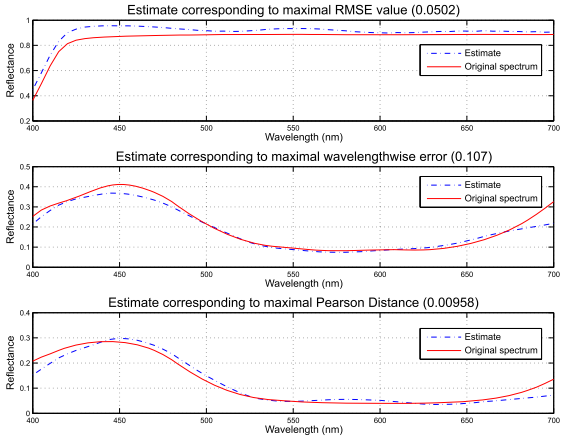

Fig. 6. Estimates for the CC24 samples (Matern kernel) corresponding to the maximal RMSE value (top); maximal wavelengthwise error (middle) and maximal Pearson Distance

5 Conclusions

We have collected a set of characterization data that can be used in the calibration of FluxData 1665 MS7 spectral video camera. We have found that small deviation in linearity exists for all channels, with channel B1 being the most non-linear. Small amount of spatial non-uniformity was found present in all the CCDs suggesting a need for a flat field image correction. No distortions were noted but only a small and systematic shift between the three sensors that can

be corrected. Separate sensor control provides possibilities for controlling and finding suitable exposure and gain values sensor-wise. At the same time the light efficiency of the trichroic prism allows for short exposure times making the system suitable for video imaging. The SNR values represent high image quality in terms of noise while sensitivity measurements show coverage of the spectral range from 380 nm to 910 nm. The spectral reflectance estimation experiments suggest reasonable accuracy for standard color charts in terms of spectral and color errors. Our experimenta resultsl suggest that camera could be suitable for several applications that require acquisition of colorimetric and spectral data via practical spectral imaging system.

References

1. Haneishi, H., Hasegawa, T., Hosoi, A., Yokoyama, Y., Tsumura, N., Miyake, Y.: System design for accurately estimating spectral reflectance of art paintings. Appl. Opt. 39, 6621–6632 (2000)
2. Kim, E.: A high-resolution multi-spectral imaging system for small satellites. Acta Astronautica 52(9-12), 813–818 (2003)
3. Thigpen, J., Shah, S., Merchant, F., Castleman, K.: Photometric Calibration for Automated Multispectral Imaging of Biological Samples. In: Proceedings of 1st Workshop on Microscopic Image Analysis with Applications in Biology (in conjunction with MICCAI, Copenhagen), pp. 27–33 (2006)
4. Antikainen, J., von und zu Fraunberg, M., Orava, J., Jääskeläinen, J.E., Hauta-Kasari, M.: Spectral imaging of neurosurgical target tissues through operation microscope. Optical Review 18(6), 458–461 (2011)
5. Eckhard, T., Valero, E.M., Hernández-Andrés, J., Heikkinen, V.: Evaluating logarithmic kernel for spectral reflectance estimation – effects on model parametrization, training set size, and number of sensor spectral channels. J. Opt. Soc. Am. A 31(3), 541–549 (2014)
6. Heikkinen, V., Mirhashemi, A., Alho, J.: Link functions and Matérn kernel in the estimation of reflectance spectra from RGB responses. J. Opt. Soc. Am. A 30(11), 2444–2454 (2013)
7. Heikkinen, V., Lenz, R., Jetsu, T., Parkkinen, J., Hauta-Kasari, M., Jääskeläinen, T.: Evaluation and unification of some methods for estimating reflectance spectra from RGB images. J. Opt. Soc. Am. A 25(10), 2444–2458 (2008)
8. Shimano, N., Terai, K., Hironaga, M.: Recovery of spectral reflectances of objects being imaged by multispectral cameras. J. Opt. Soc. Am. A 24, 3211–3219 (2007)